Journal of Catalysis **183,** 373–383 (1999)
Article ID jcat.1999.2408, available online at http://www.idealibrary.com on IDEAL®

Cobalt-Catalyzed Amination of 1,3-Propanediol: Effects of Catalyst Promotion and Use of Supercritical Ammonia as Solvent and Reactant

A. Fischer, M. Maciejewski, T. Bürgi, T. Mallat, and A. Baiker[1]

Laboratory of Technical Chemistry, Swiss Federal Institute of Technology, ETH-Zentrum, CH-8092 Zurich, Switzerland

Received November 16, 1998; revised December 22, 1998; accepted December 22, 1998

The catalytic synthesis of 1,3-diaminopropane from 1,3-propanediol and ammonia was studied in a continuous fixed-bed reactor in the pressure range 50 to 150 bar. The unsupported Co-based catalysts applied were characterized by N_2 physisorption, XRD, XPS, TPR, and ammonia adsorption using pulse thermal analysis and DRIFT spectroscopy. The latter investigations revealed that the best catalyst, 95 wt% Co–5 wt% Fe, contained only very weak acidic sites, unable to chemisorb ammonia. The absence of strong acidic and basic sites was crucial to suppress the various acid/base-catalyzed side reactions (retro-aldol reaction, hydrogenolysis, alkylation, disproportionation, dimerization, oligomerization). Other important requirements for improved diaminopropane formation were the use of excess ammonia (molar ratio NH_3/diol > 20) and the presence of the metastable β-Co phase. A small amount of Fe additive could efficiently hinder the transformation of this phase into the thermodynamically stable α-Co phase and thus prevent catalyst deactivation up to 10 days on stream. Application of supercritical ammonia almost doubled the selectivity to amino alcohol and diamine. The selectivity enhancement in the near-critical region is attributed to elimination of the interphase mass transport limitations and to the resulting higher surface ammonia concentration.

Key Words: **amination; α-cobalt; β-cobalt; 1,3-diaminopropane; 1,3-propanediol; supercritical ammonia; effect of iron and lanthanum promotion.**

INTRODUCTION

Amination of aliphatic alcohols for the synthesis of aliphatic amines is an industrially relevant process. Numerous examples with good to high yields can be found in reviews and books (1–12). The reaction is catalyzed by metal hydrogenation–dehydrogenation-type catalysts such as nickel, cobalt, and copper and by solid acids (mainly zeolites and phosphates).

In comparison to reports on the amination of simple aliphatic alcohols, studies on the transformation of diols to the corresponding acyclic primary amines are scarce and presented mainly in the patent literature (13–18). The information available in patents provides only little insight into this type of amination reactions. A typical example is the amination of 1,3-propanediol with NH_3, which was chosen to illustrate the application range of a nickel–rhenium catalyst (17, 18). There are no data available concerning the product composition, except the conversion (45%) estimated on the basis of water formed.

Amination of a simple aliphatic alcohol over a metal catalyst is already a complex process which consists of dehydrogenation, condensation, and hydrogenation steps (Scheme 1) (12, 19). The first and last redox processes are catalyzed by the metal, while the reaction of the intermediate carbonyl compound with NH_3 or an amine to form an imine or enamine does not require a metal catalyst, but can be accelerated by acid/base catalysis (12, 20). Each intermediate and the product amine can take part in various side reactions [for details, see (1, 4, 7, 11, 12)]. The synthesis of a diamine from the corresponding diol requires repetition of the three major steps which multiplies the likelihood of undesired side reactions, including oligomerization and cyclization (21–23).

A further complication in the synthesis of primary amines is that the product amines are significantly more reactive than the reagent NH_3. This effect may be illustrated by the amination of 1,6-hexanediol. When using NH_3, only 23% 1,6-diaminohexane was obtained at 220°C and 300 bar (16). Amination with dimethylamine ran smoothly at atmospheric pressure and 195°C, affording 51% of the corresponding diamine (24).

We have recently found that the application of supercritical ammonia ($scNH_3$) as a solvent and reactant provides a remarkable selectivity improvement in the amination of aliphatic diols, compared with the performance of the same catalyst under similar conditions, but applying subcritical pressures (25). The aim of the present work was to obtain deeper insight into this demanding type of amination reaction and reveal the role of the catalyst in controlling the product distribution. From economic and environmental points of views, the direct synthesis of aliphatic diamines

[1] To whom correspondence should be addressed.

0021-9517/99 $30.00

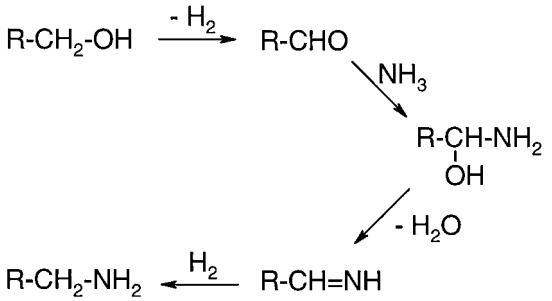

SCHEME 1

from diols and NH_3 would be an attractive alternative to the presently applied methods (3, 26, 27).

EXPERIMENTAL

Materials

1,3-Propanediol (>97%, Fluka), 3-amino-1-propanol (>98%, Fluka), NH_3 (99.98%, Pan-Gas), H_2 (99.999%, Pan-Gas), and N_2 (99.995%, Pan-Gas) were used without further purification.

Important properties of the various cobalt-based catalysts used are collected in Table 1. Distilled water was applied in all catalyst preparations. According to a general procedure, the metal nitrates were dissolved in 500 ml water. About 100 g of an aqueous solution containing 20 wt% $(NH_4)_2CO_3$ was then dropped into the metal nitrate solution over 1 h at room temperature until a pH of 7 was reached. After 2 h stirring the precipitate was filtered, washed, and dried at 100°C at reduced pressure (<10 kPa). The material was calcined in air at 400°C for 2 h, mortared, and sieved to a particular mesh size (0.14–0.4 mm). Subsequently the sample was activated in the reactor by reduction with H_2 for 4 h at 335–420°C (Table 1). The reduction temperature was chosen based on the maximum H_2 consumption rate in TPR (see Table 2).

TABLE 1

Preparation of Various Cobalt-Based Catalysts

Catalyst	Metal content[a] (wt%)	Precursor (mmol)	Reduction temperature (°C)
Co	Co(100)	$Co(NO_3)_2 \cdot 6\,H_2O$(172)	335
Co–La	Co(88), La(12)	$Co(NO_3)_2 \cdot 6\,H_2O$(171) $La(NO_3)_3 \cdot 6\,H_2O$(9.2)	335
Co–Fe	Co(95), Fe(5)	$Co(NO_3)_2 \cdot 6\,H_2O$(171) $Fe(NO_3)_3 \cdot 9\,H_2O$(9.2)	335
Co–Fe-48	Co(52), Fe(48)	$Co(NO_3)_2 \cdot 6\,H_2O$(171) $Fe(NO_3)_3 \cdot 9\,H_2O$(9.2)	340
Co–Fe–PO_4	Co(95), Fe(5)[b]	$Co(NO_3)_2 \cdot 6\,H_2O$(171) $Fe(NO_3)_3 \cdot 9\,H_2O$(9.2) $(NH_4)_2HPO_4$[c]	420
Co–Fe–Na	Co(95), Fe(5)[b]	$Co(NO_3)_2 \cdot 6\,H_2O$(171) $Fe(NO_3)_3 \cdot 9\,H_2O$(9.2) NaOAc[c]	335

[a] Determined by ICP-AES.

[b] Bulk PO_4^{3-} and Na^+ contents were minor; for surface composition see Table 3.

[c] Co–Fe catalyst "precipitate" was treated with aqueous $(NH_4)_2HPO_4$ or NaOAc solutions before drying and calcination.

Two fractions of the wet precipitate of the Co–Fe catalyst (Table 1) were additionally treated with sodium acetate or ammonium hydrogen phosphate, to modify their acid/base properties. For this purpose, ca. 68 g of the wet hydrated oxide–carbonate was mixed with 100 ml 0.1 M aqueous NaOAc or $(NH_4)_2HPO_4$ solution. The slurry was mixed at 90°C for 30 min, filtered, and washed carefully with hot water. The following steps were identical to those of the general procedure.

Catalyst Characterization

Specific surface areas (S_{BET}), mean cylindrical pore diameters ($\langle d_p \rangle$), and specific pore volumes ($V_{p(N_2)}$) were determined by N_2 physisorption at 77 K using a Micromeritics ASAP 2000 apparatus. Catalyst samples were first degassed for 10 h at 100°C. The surface area was calculated in the relative pressure range 0.05 to 0.2, assuming a cross-sectional area of 0.162 mm^2 for the N_2 molecule. The mean cylindrical pore diameter was determined using the relation $\langle dp \rangle = 4V_{p(N_2)}/S_{BET}$.

X-ray diffraction patterns were obtained on a Siemens D5000 powder X-ray diffractometer using Cu$K\alpha$ radiation (35 mA, 35 mV, Ni filter).

XPS measurements were performed with a Leybold Heraeus LHS11 apparatus using MgKα radiation. The work function of the spectrometer was set so that the Au $f_{7/2}$ line for metallic gold was located at 84.0 eV. Thin sample films were pressed on a sample holder, evacuated in a load lock, and subsequently transferred into the UHV chamber for analysis. Pass energies of 151 and 63 V were used. Slight sample charging was corrected using the C 1*s* line at 284.6 eV as an internal standard. Differential charging was estimated by varying the potential of a tubus in the lens system of the analyzer.

Adsorption of NH_3 was studied using the pulse thermal analysis technique on a Netzsch STA 409 thermal analyzer (28, 29). NH_3 pulses were injected with a Valco dual external sample injection valve equipped with two 1-ml sample loops. A quadrupole mass spectrometer (QMG 420, Balzers) was used for analysis of the gas composition. After calcination and reduction of the catalyst, NH_3 pulses were injected into the He carrier gas flow of 50 ml min^{-1}, under isothermal conditions.

The same thermal analyzer system was used for determining the TPR profiles. Eighty milligrams of catalyst was heated in a flow of 10% H_2 in He, at a heating rate of 5 K min^{-1}. The formation of water (product of catalyst re-

TABLE 2

Structural Properties of the Co-Based Catalysts Determined by N_2 Physisorption, TPR, and XRD Analysis

Catalyst	Calcination (°C)	S_{BET}[a] ($m^2\ g^{-1}$)	V_{p,N_2}[b] ($cm^3\ g^{-1}$)	$\langle d_p \rangle$[c] (nm)	T_{TPR}[d] (°C)	Phases detected by XRD (crystallite size in nm)[e]
Co	400	54	0.34	21	338	CoO(12), Co_3O_4(22)
Co–La	400	37	0.43	34	356	Co_3O_4(16)
Co–Fe[f]	—	108	0.58	14	—	Poorly crystalline
Co–Fe	400	35	0.31	29	383	CoO(25), Co_3O_4(22)
Co–Fe[g]	400	12	0.10	43	—	β-Co(31)
Co–Fe[h]	400	6	0.02	15	—	β-Co(31)
Co–Fe-48	400	68	0.15	7	401	Poorly crystalline
Co–Fe–PO_4	400	133	0.67	17	492	Co_3O_4(13)
Co–Fe–Na	400	91	0.6	23	397	Co_3O_4(16)

[a] BET surface area.
[b] BJH cumulative desorption pore volume.
[c] Mean pore diameter $\langle d_p \rangle = 4V_{p,N_2}/S_{BET}$.
[d] Temperature of maximum hydrogen consumption.
[e] Mean crystallite size determined by XRD line broadening.
[f] Without calcination.
[g] Calcined and reduced.
[h] After amination reaction.

duction) was monitored by MS. For investigating the decomposition of NH_3, 60 mg Co–Fe catalyst, prereduced in H_2 in a preceding cycle, was heated in a flow of 10% NH_3 in He at the heating rate of 10 K min^{-1}.

The chemical composition of the catalysts was determined by ICP-AES using an IRIS ICP-AES spectrometer (Thermo Jarell Ash) in an inductively coupled Ar plasma chamber.

DRIFT spectroscopic measurements were carried out on a Perkin–Elmer 2000 FTIR spectrometer. A KBr background spectrum was recorded at 50°C (100 scans with a resolution of 1 cm^{-1}) after heating the sample for 1 h in an Ar flow of 15 ml min^{-1}. The catalyst was pretreated at 300°C for 1 h in Ar to remove physisorbed water. Subsequently, the sample was reduced with H_2 at the same temperature as applied before the catalytic tests (see above). The background spectrum of the sample was recorded in Ar at temperature steps of 50°C from 50 to 250°C. After being cooled to 50°C, the catalyst was flushed with NH_3 (3600 ppm in Ar, 50 ml min^{-1}) for 20 min. Spectra were recorded at temperature steps of 50°C from 50 to 250°C.

Catalytic Amination

The apparatus consisted essentially of a dosing system for the reactants, a high-pressure fixed-bed reactor, and a gas/liquid separator. The reactor was constructed of Inconel-718 tubing of 13-mm inner diameter and 38-ml volume. The temperature in the reaction zone was measured with a thermocouple located in the center of the tube and was regulated with a PID cascade controller. Total pressure in the reactor system was set by a Tescom backpressure regulator. Liquid NH_3 and 1,3-propanediol were dosed with syringe pumps (ISCO D500). The reactor was operated in down flow mode. Standard conditions used were 8.0 g catalyst, 195°C, 135 bar, contact time 40,000 gs mol^{-1}, molar ratio of propanediol/NH_3/H_2-1/60/2.

Concentrations in the liquid product mixture were determined by GC analysis using external calibration standards (HP-5890A, FID detector, HP-1701 capillary column). Losses of the desired products due to possible evaporation were minor, as confirmed in specific experiments. Individual products were identified by GC–MS analysis.

A 50-ml high-pressure quartz cell was used to investigate whether the reaction mixture was in the supercritical state. The experiment was performed with a mixture consisting of propanediol/NH_3/H_2 at a molar ratio of 1/60/2. Visual inspection of the phase behavior at 130 bar and 200°C confirmed the existence of a substantially homogeneous supercritical phase. Note that the critical data on pure NH_3 are $T_c = 132.4$°C and $P_c = 114.8$ bar (30). Conversion of alcohol X_a and selectivity S_i of product amine i were defined as

$$X_a = 100 * (F_{a0} - F_a)/F_{a0},$$
$$S_i = F_i/(F_{a0} - F_a),$$

where F_{a0} and F_a correspond to molar flow rates of diol at reactor inlet and outlet, respectively, and F_i represents the molar flow rate of product i at reactor outlet.

RESULTS

Catalyst Characterization

Textural properties and surface composition of the calcined catalysts. Some important properties of the Co-based catalysts, obtained by N_2 physisorption, TPR, and XRD methods, are summarized in Table 2. All uncalcined

catalysts were poorly crystalline. During calcination the surface area and pore volume decreased considerably, as emerges from the comparison of Co–Fe and Co–Fe[f] (Table 2). The unsupported materials after calcination possessed relatively high surface areas up to 133 $m^2 g^{-1}$. Addition of Fe or La to Co as a second component changed considerably the pore volume, pore diameter, and surface area. Similarly, treatments of Co–Fe after precipitation and before drying with ammonium hydrogen phosphate (Co–Fe–PO_4) or sodium acetate (Co–Fe–Na) had a remarkable influence on the textural properties.

X-ray patterns of the calcined catalysts showed the presence of cobalt oxides, mainly Co_3O_4. The CoO phase was absent after addition of 5 wt% La or treatments with NaOAc or $(NH_4)_2HPO_4$.

XPS analysis of Co–Fe–Na and Co–Fe–PO_4 confirmed the existence of Na and P, respectively, on the surface of the modified Co–Fe catalysts. Sodium was identified by the peak at 1071.1 eV (Na 1*s*) and phosphorus by the signal at 132.5 eV (P 2*p*) which is indicative of phosphate (31). The $2p_{3/2}$ line of cobalt was found at a binding energy of 780.17 eV, consistent with Co_3O_4 or Co_2O_3 (32, 33). Only weak shakeup satellites for the $2p_{3/2}$ line indicated mostly diamagnetic Co(III). The Fe $2p_{3/2}$ line at 710.5 eV is characteristic of Fe_3O_4 or Fe_2O_3 (33).

The surface composition was estimated by integrating the XPS signals of the different elements using formerly determined sensitivity factors (34). The results are listed in Table 3. The relative abundance of iron to cobalt at the surface of the Co–Fe catalyst was almost twice as great as in the bulk (determined by ICP-AES, see Table 1). The materials treated with sodium acetate or ammonium hydrogen phosphate exhibited about the same Co/Fe ratio at the surface as in the bulk.

Characteristics of the reduced catalysts. Amination of alcohols over metal catalysts is catalyzed by surface M^0 sites. The calcined catalysts, which can only be considered as "precursors" of the real active materials, were prereduced *in situ* before use. The reducibility of various Co-based mono- and bimetallic catalysts and the influence of treatments with acidic or basic salts were studied by temperature-programmed reduction. Three examples are shown in Fig. 1. The shapes of the reduction curves of Co–Fe

TABLE 3

XPS Analysis (in at.%) of Some Unreduced Co–Fe Catalysts

Catalyst	Element (sensitivity factor)			
	Co 2*p*(3.8)	Fe 2*p*(3.0)	Na 1*s*(2.3)	P 2*p*(0.39)
Co–Fe	45.2	4.5	—	—
Co–Fe–Na	45.4	2.5	2.7	—
Co–Fe–PO_4	44.5	2.3	—	5.7

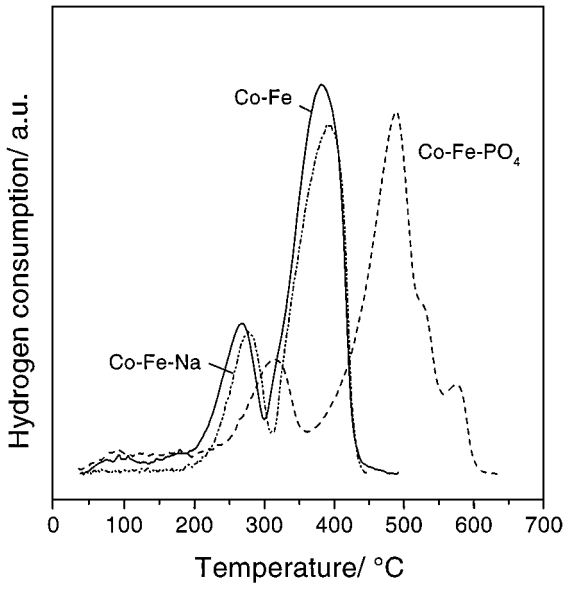

FIG. 1. Temperature-programmed reduction of calcined Co–Fe, Co–Fe–PO_4, and Co–Fe–Na catalysts. Conditions: 10% H_2 in He, heating rate 5°C min^{-1}, gas flow rate 50 ml min^{-1}.

and Co–Fe–Na are similar to that obtained for the calcined sample containing only Co. The weight loss observed during reduction indicated that the two peaks represent the reduction of Co_3O_4 to Co via CoO (35). Reduction of Co–Fe–PO_4 (and also Co–Fe-48) occurred in three steps. The maxima of the biggest peaks of all catalysts are shown in Table 2. TPR measurements confirmed that temperatures listed in Table 1 for catalyst prereduction before amination were sufficiently high to complete the reduction of oxides to metals.

In additional sets of TPR experiments, NH_3 (10 vol% in He) was applied as a reducing agent. The reduction started above 250°C and all peaks were shifted to higher temperatures, compared with the runs in which H_2 was used. For example, with Co–Fe the maximum in the TPR signal was shifted from 383 to 470°C. The experiment with Co–Fe was repeated with the prereduced catalyst to determine unambiguously the temperature range in which the metals are active in NH_3 decomposition. This reaction, indicated by the formation of H_2, was observed only from 250°C onward. Therefore, decomposition of NH_3 as a side reaction during catalytic amination of propanediol at or below 210°C (see later) can be excluded.

The phase composition of Co after prereduction and after the amination reaction is shown in Fig. 2. After reduction with H_2 at 335°C, the catalyst consisted of hexagonal close-packed α-Co and face-centered cubic β-Co (Fig. 2a). At moderate temperatures β-Co is metastable, which explains the growth of the main reflection of the α-Co phase at 47.5° (Fig. 2b) during the amination reaction (at 150–210°C for 12 h). Previous XRD studies on Co catalysts ascertained

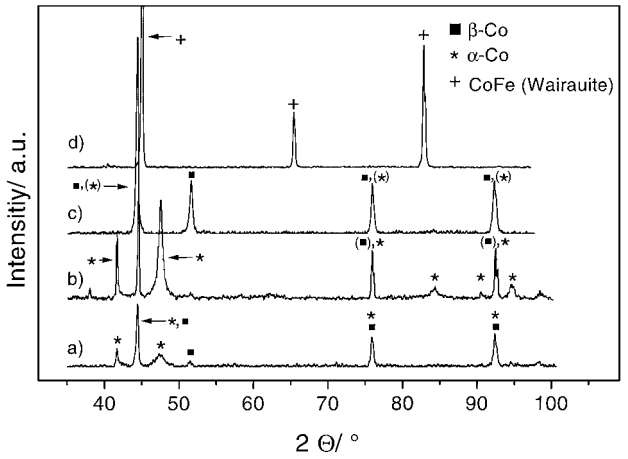

FIG. 2. X-ray diffraction patterns of Co (a), Co–Fe (c), and Co–Fe-48 (d) after calcination and reduction, and Co (b) after use in amination.

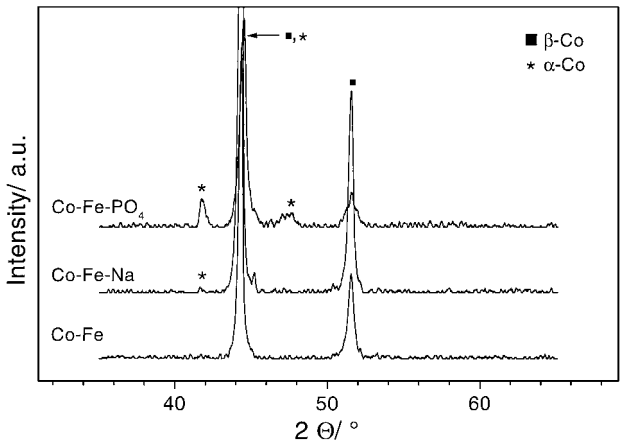

FIG. 3. X-ray diffraction patterns of Co–Fe, Co–Fe–PO_4, and Co–Fe–Na after calcination and reduction.

the importance of the reduction temperature in the development of α and β phases. Only β-Co was generated by H_2 reduction at 400°C (36). The sluggish transition from α- to β-Co was observed between 340 and 380°C (37).

Figures 2c and 2d illustrate the influence of Fe additive on the phase composition of the reduced catalysts. Interestingly, only β-Co was detectable when the catalyst containing 5 wt% Fe (Co–Fe) was reduced at 335°C. At this temperature formation of the α-Co phase is expected (37). Apparently, the presence of Fe favored formation of the metastable β-Co phase. Moreover, restructuring during the amination reaction was suppressed and the β-Co phase was still present after use at 150–210°C for 10 days (not shown in Fig. 2). The average size of Co crystallites in reduced Co–Fe remained unaffected during the amination reaction (see Co–Fe^g and Co–Fe^h in Table 2). Similarly, addition of 5 wt% La to Co prevented the restructuring of Co during amination; these results are not shown here. These experimental observations reflect the excellent stabilizing effect of a small amount of Fe or La additive. An increase in the iron content to 48 wt% (Co–Fe-48) resulted in the development of a new phase, a CoFe alloy (Wairauite), during reduction by H_2.

A partly different picture was obtained in the study of Co–Fe catalysts treated with basic or acidic salts. The XRD patterns of Co–Fe–Na (reduced at 335°C) and Co–Fe–PO_4 (reduced at 440°C) disclosed the presence of both cobalt phases, though the amount of α-Co was very small in Co–Fe–Na (Fig. 3). Structural changes during amination were not observed for any of these two catalysts.

Adsorption of ammonia. Pulse thermal analysis (PTA) was used for the quantitative study of NH_3 physisorption and chemisorption. This method provides correct, undistorted values by following the weight change during adsorption and desorption (28, 29). The data measured on the reduced samples of Co–Fe, Co–Fe–PO_4, and Co–Fe–Na at 50°C are collected in Table 4. The amount of NH_3 physisorbed on Co–Fe was small and it was completely removed by the He carrier gas within 5 min. Besides, no chemisorbed NH_3 could be detected. A combined UPS and XPS study revealed earlier that the adsorption of NH_3 on Co is very weak at room temperature (38).

Co–Fe–PO_4 was the only catalyst that chemisorbed NH_3. Its desorption occurred between 75 and 250°C, with a maximum rate at 170°C. Chemisorption of NH_3 is a clear indication for acidic sites introduced by the treatment with $(NH_4)_2HPO_4$. The enhanced capacity for physisorbed NH_3 of this catalyst may simply be attributed to the higher surface area, as compared with the untreated Co–Fe catalyst (Table 4). On the other hand, neither physisorption nor chemisorption of NH_3 could be detected on Co–Fe–Na, as expected for this base-treated material.

To our knowledge, no report has yet appeared on the DRIFT study of NH_3 adsorption on Co. Due to the lack of a reference spectrum, DRIFT spectra of NH_3 adsorbed on Ni and Cu catalysts were used to allocate the adsorption bands (39–41). Figure 4 shows the spectra of NH_3 chemisorbed on the prereduced Co–Fe–PO_4 catalyst at different temperatures. Adsorbed NH_3 could be detected up to 250°C. Vibrations at 1240 and 1610 cm^{-1} are ascribed to Lewis acid centers (δ_s NH_3, δ_{as} NH_3). The weaker deformation mode at

TABLE 4

Ammonia Adsorption Determined by Pulse Thermal Analysis at 50°C, Together with the BET Surface Areas

Catalyst	Physisorption ($cm^3\,g^{-1}$)	Chemisorption ($cm^3\,g^{-1}$)	S_{BET} ($m^2\,g^{-1}$)
Co–Fe	0.4	0	12
Co–Fe–PO_4	0.8	1.5	31
Co–Fe–Na	0	0	6

[a] Both measurements were carried out on catalysts prereduced by H_2.

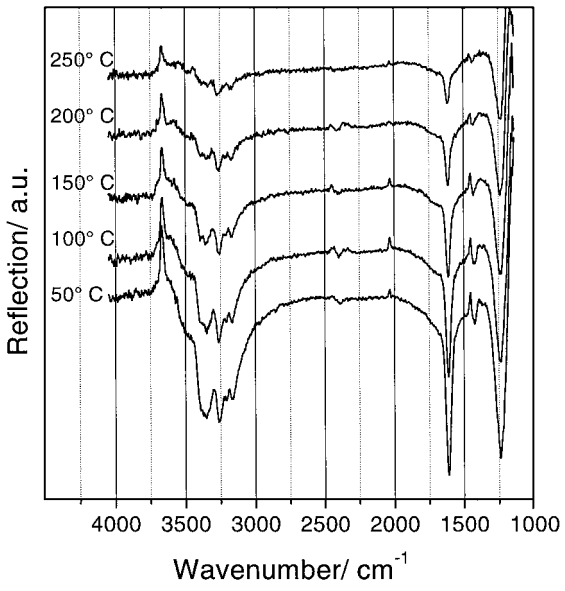

FIG. 4. DRIFT spectra of adsorbed ammonia on the reduced Co–Fe–PO_4 catalyst at different temperatures. Carrier gas: 50 ml min^{-1} Ar. Spectra obtained after subtraction of the background spectrum are shown.

1423 cm^{-1} is attributed to Brønsted populations (δ_{as} NH_4^+). The weak δ_s NH_4^+ around 1670 cm^{-1} could not be clearly identified. A multiplet was observed in the NH stretching region (3352 cm^{-1}, 3258 cm^{-1}, 3216 cm^{-1}, 3165 cm^{-1}) that is assigned to the asymmetric and symmetric νN–H and to the first overtone of $2\delta_{as}$ NH_3 vibrations (42). The reverse adsorption signal at 3668 cm^{-1} indicates a decrease in the amount of hydroxyl groups on the catalyst surface, because NH_3 was adsorbed on Brønsted sites.

With increasing temperature NH_3 desorbed from the surface and the intensity of the signals decreased. No chemisorbed NH_3 could be detected on the surface of Co–Fe and Co–Fe–Na catalysts, in agreement with the PTA experiments (Table 4).

Catalytic Amination

Choice of catalyst. Screening of several supported and unsupported metal catalysts in an autoclave revealed that only Co-, Ni-, and Cu-based catalysts were useful for the amination of 1,3-propanediol. Ru/C and Pd/C were active but unselective.

A parameter study was carried out in the fixed-bed reactor with the most promising catalysts Co, Co–La, and Co–Fe. It was found that a small proportion of H_2 in the feed (1–5 mol%) was sufficient to prevent the undesired dehydrogenation reactions leading to the formation of nitriles and carbonaceous deposits (43). For the comparison of Co, Co–Fe, and Co–La catalysts the pressure was set at 135 bar and the temperature was varied between 190 and 210°C. Note that NH_3 forms a supercritical fluid above $T_c = 132.4$°C and $P_c = 114.8$ bar (30). A rather high molar excess of NH_3 was employed to minimize oligomerization of the intermediates and products. The existence of a substantially homogeneous supercritical reaction mixture was confirmed by separate experiments in a quartz cell (see Experimental). Some representative data illustrating the activity and selectivity of Co-based catalysts are listed in Table 5. A considerable deactivation within 12 h on stream was observed with unpromoted Co. It is likely that deactivation is connected to the restructuring of Co, as observed by XRD (Figs. 2a and 2b).

Restructuring was negligible with bimetallic catalysts containing 5 wt% Fe or La. Conversion and selectivity values presented in the following figures and tables could be

TABLE 5

Catalyst Screening Tests for the Amination of 1,3-Propanediol[a]

Catalyst	Temperature (°C)	Molar ratio diol/NH_3/H_2	Conversion (%)	Selectivity (%)	
				Aminol (**3**)	Diamine (**4**)
Co[b]	210	1/20/2	90	6	11
Co[c]	210	1/20/2	58	26	21
Co[b]	195	1/60/2	98	5	12
Co–La	190	1/20/2	36	31	12
Co–La	210	1/20/2	80	12	11
Co–La	210	1/60/2	98	5	23
Co–Fe	210	1/20/2	94	0	11
Co–Fe	195	1/60/2	95	9	34
Co–Fe-48[d]	195	1/60/2	42	14	7
Co–Fe-48[e]	195	1/60/2	96	<3	<3

[a] Conditions: 135 bar, contact time: 60,000 gs mol^{-1}.
[b] Values were determined after 3 h time on stream.
[c] Values were determined after 12 h time on stream.
[d] Contact time: 40,000 gs mol^{-1}.
[e] Contact time: 100,000 gs mol^{-1}.

reproduced after 6–12 h on stream. Accordingly, Co–La and Co–Fe were chosen for further investigations.

Product distribution. On the basis of the major components identified in the liquid product mixture by GC–MS analysis, the important reactions occurring during amination of 1,3-propanediol are depicted in Scheme 2. Besides the key intermediate amino alcohol **3** and product diamine **4**, various compounds have been detected that formed by fragmentation (**7**, **8**), alkylation (**9**, **10**, **14**), and dimerization (**11**–**13**). The retro-aldol reaction via the β-hydroxyaldehyde **2** (21) produced reactive carbonyl compounds (**5** and **6**). These aldehydes could not be detected in the liquid product mixture, likely due to their high reactivity and volatility. Their existence was deduced from the formation of alkylation products **9** and **10**. The ratio of main to by-products varied strongly with the reaction conditions, as shown below.

Influence of reaction parameters. Figure 5 depicts the influence of temperature on the conversion of 1,3-propanediol and on the yields of some key products over Co–Fe. The conversion of 1,3-propanediol, which indicates the consumption of the diol via the formation of a β-hydroxy-

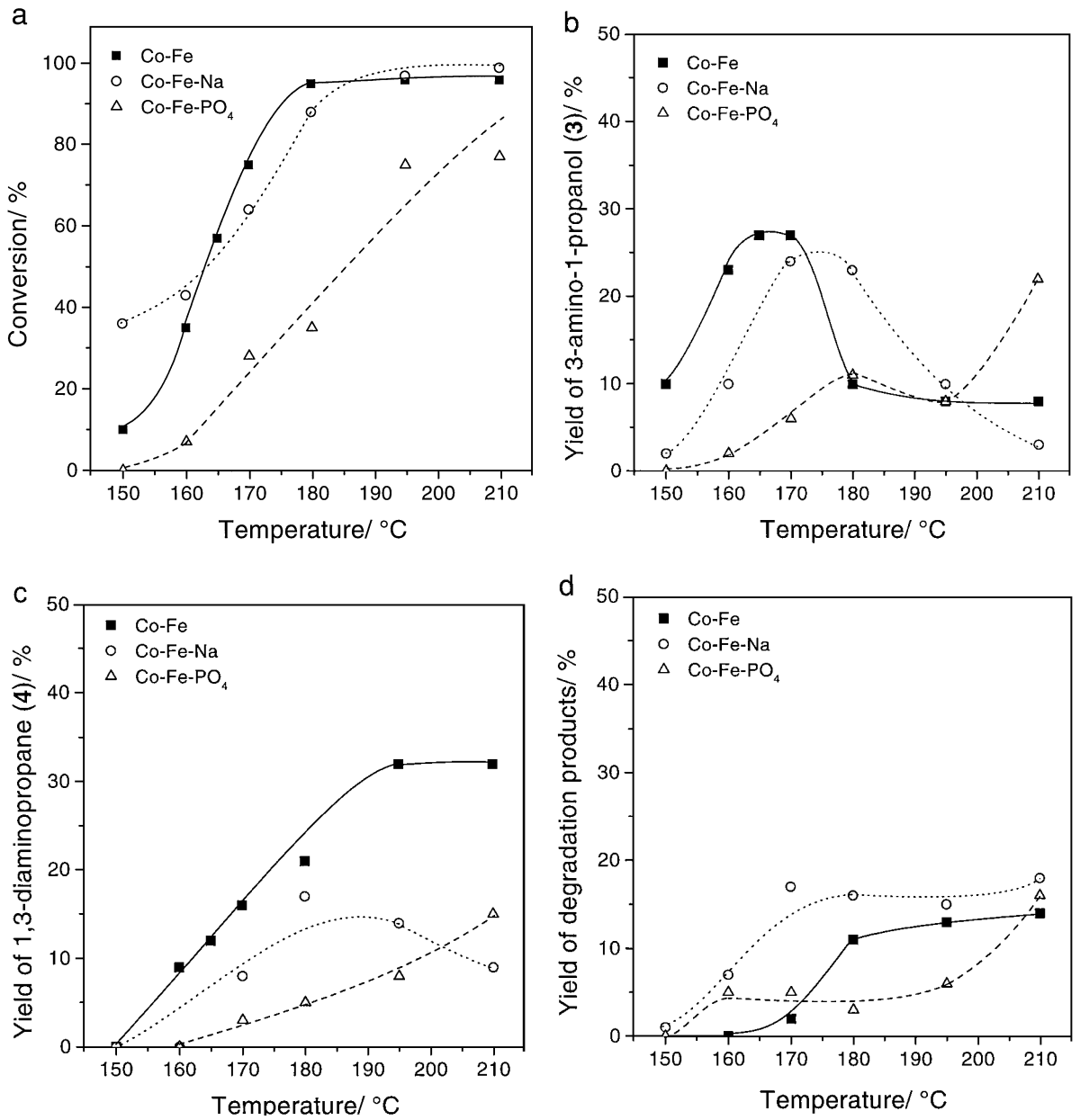

FIG. 5. Influence of temperature on the conversion of 1,3-propanediol (a) and on the yields of **3** (b), **4** (c), and degradation products **7**–**10** (d) over Co–Fe, Co–Fe–Na, and Co–Fe–PO_4. Standard conditions.

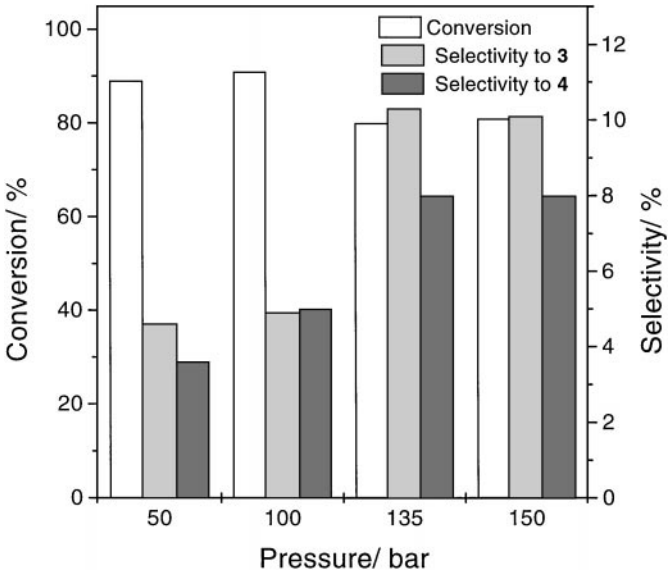

FIG. 6. Effect of total pressure on the amination of 1,3-propanediol over Co–La. Conditions: 210°C, reactant molar ratio (diol/NH_3/H_2): 1/20/2; contact time: 60,000 gs mol^{-1}.

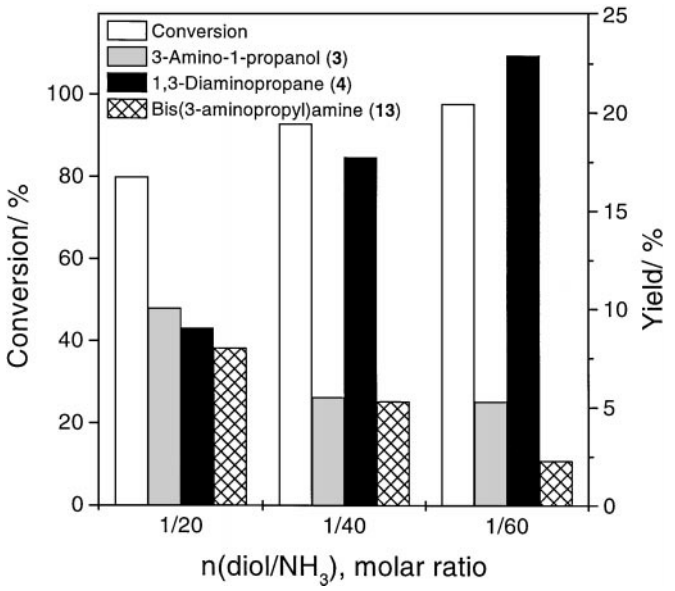

FIG. 7. Influence of NH_3/diol molar ratio on the conversion of 1,3-propanediol and product distribution over Co–La. Conditions: 210°C, contact time: 60,000 gs mol^{-1}; otherwise standard conditions.

aldehyde **2**, increased by an order of magnitude in the temperature range 150–180°C. The variation in the yields of amino alcohol **3**, diamine **4**, and degradation products **7**–**10** with temperature is typical of a consecutive reaction series.

The effect of total pressure on the product distribution is illustrated with the results obtained over the Co–La catalyst (Fig. 6). There is a remarkable enhancement in selectivities to **3** and **4** in the range of the subcritical–supercritical transition of NH_3 [$P_c = 114.8$ bar (30)]. The change in selectivity was minor below 100 bar and above 135 bar, and the variation in conversion was small over the whole pressure range. It has been proved independently that at 200°C and 130 bar the reaction mixture was in a homogeneous supercritical phase.

The influence of NH_3/diol molar ratio is shown in Fig. 7. The higher this ratio, the higher are the conversion of diol **1** and the cumulative selectivity for aminol **3** and diamine **4**. Simultaneously, the formation of dimers **11**–**13** was diminished, which is illustrated by the example of **13**. As discussed in the Introduction, the reactivity (basicity) of NH_3 is markedly lower than that of the primary amines produced. This reactivity difference leads to the formation of various dimerization and oligomerization products (the aldehyde intermediate reacts with an amine, instead of NH_3, to produce a secondary amine). A relatively large NH_3/diol molar ratio (>20) is necessary to compensate this effect and improve the selectivities to primary amines. A large excess of NH_3 also favors the condensation of NH_3 with the aldehyde intermediate **2** by shifting the equilibrium toward the adduct, and suppresses the disproportionation of primary amines to secondary amines and NH_3 (1, 4, 12).

Product distribution was strongly affected by the contact time, as shown in Fig. 8. Longer contact times increased the conversion and decreased the selectivities for **3** and **4**. However, the yields of these products (i.e., conversion times selectivity) remained almost constant. Interestingly, working with a short contact time at higher temperature (20,000 gs mol^{-1}, 210°C, see Fig. 8), or with a longer contact time at lower temperature (60,000 gs mol^{-1}, 190°C, see Table 5)

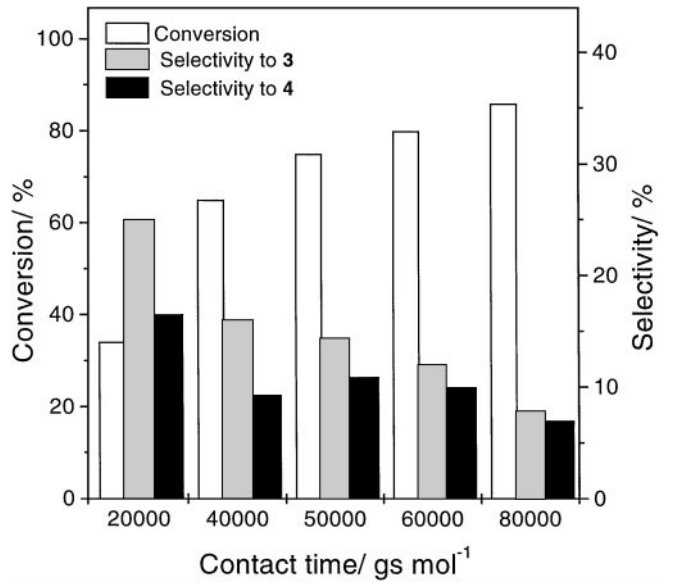

FIG. 8. Effect of contact time on conversion of 1,3-propanediol (**1**) and selectivities for 3-amino-1-propanol (**3**) and 1,3-diaminopropane (**4**) over Co–La. Conditions: 210°C, reactant molar ratio (diol/NH_3/H_2): 1/20/2; otherwise standard conditions.

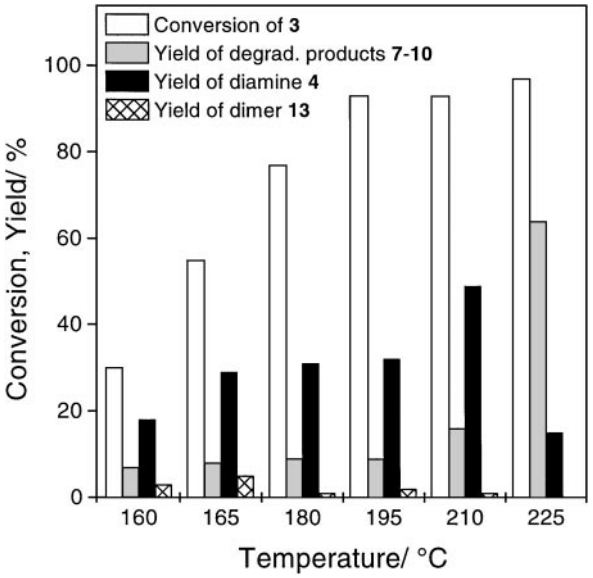

FIG. 9. Influence of temperature on the amination of 3-amino-1-propanol (**3**) over Co–Fe. Standard conditions.

afforded almost identical conversions (34–36%) and cumulative selectivities for **3** and **4** (43%). Attempts to improve the diamine yield at high diol conversion by varying either the temperature or the contact time resulted in rather similar values.

*Amination of 3-amino-1-propanol (**3**).* Each intermediate and the product amine can take part in various side reactions, as shown in Scheme 2. In a series of experiments the amination of the key intermediate 3-amino-1-propanol (**3**) was investigated. Starting from this intermediate instead of **1**, the number of necessary reaction steps is halved and the selectivity to the diamine **4** is expected to rise considerably. The results shown in Fig. 9 confirm this expectation. The maximal yield of 50% **4** was remarkably higher than the best value of 32% achieved under similar conditions in the amination of the diol **1** (Fig. 5c). In both reactions, in the amination of **1** and **3**, the drop in diamine yield above 210°C is due mainly to the enhanced formation of degradation products (see Fig. 9 as an example).

Catalytic performance of Co–Fe treated with NaOAc or $(NH_4)_2HPO_4$. The effect of basic and acidic treatments of Co–Fe on propanediol conversion and product distribution is shown in Fig. 5. Introduction of acidic sites by the phosphate treatment resulted in significant deactivation. A clear indication is the lower conversions by 20–60% achieved at 150–210°C, as compared with the performance of unmodified Co–Fe (Fig. 5a). Similarly, the maximum in yields for **3** and **4** was shifted to higher temperatures (≥210°) (Figs. 5b, 5c). A possible explanation for the observed deactivation is that in part, metal phosphates were formed on the catalyst surface during calcination, and in the amination of alcohols phosphates require markedly higher temperatures than metal catalysts (44, 45).

Treatment with NaOAc was less detrimental to the formation of the amino alcohol intermediate, but the diamine yield dropped above 180°C due to various side reactions, mainly degradation (Fig. 5d).

DISCUSSION

Influence of Supercritical Ammonia

The one-step amination of 1,3-propanediol (**1**) to 1,3-diaminopropane (**4**) was studied over Co-based catalysts under conditions where ammonia forms a supercritical medium (above 132.4°C and 114.8 bar). At best, a 95 wt% Co–5 wt% Fe catalyst (Co–Fe) afforded 32% diamine yield at almost complete conversion. Compared with the amination of simple monofunctional alcohols with NH_3 over metal catalysts, this result is rather moderate (8, 46). However, excluding our work, there is no other report in the open literature on the successful amination of **1**. The likely reason is not lack of interest in the product diamine, which is a useful and versatile intermediate (3). Rather the complexity of the process—eight major reaction steps including many more elementary steps—hampers any easy success in the production of **4**.

The application of $scNH_3$ as reactant and reaction medium has been found to be essential for obtaining reasonable selectivities. A change from subcritical to supercritical conditions by increasing the total pressure almost doubled the selectivity to the amino alcohol intermediate **3** and diamine **4** over Co–La (Fig. 6). An even more pronounced influence of pressure was observed over the more selective Co–Fe catalyst (25). The existence of a single supercritical phase (instead of liquid and gas phases) eliminated the interphase mass transfer resistance (47, 48). It is very likely that the positive changes in amination selectivity in the near-critical region are due to the increased surface NH_3 concentration. Analysis of the main and side reactions in Scheme 2 suggests that high surface NH_3 concentration favors the desired reaction series leading to **4** and suppresses several side reactions including dimerization, oligomerization, disproportionation, retro-aldol reaction, and hydrogenolysis.

Promotion of Co with La and Fe

The proper choice of catalyst was also important in achieving reasonable and reproducible yields of **4**. The best catalyst was developed by promoting Co with 5 wt% Fe. La as additive was less efficient. The stability of the Co–Fe catalyst is remarkable: no significant deactivation was observed even after 10 days of use at 150–210°C.

Only the metastable β-Co phase formed during reduction prior to the amination reaction, and no detectable restructuring occurred over several days on stream. For comparison, unpromoted Co, which was less selective and

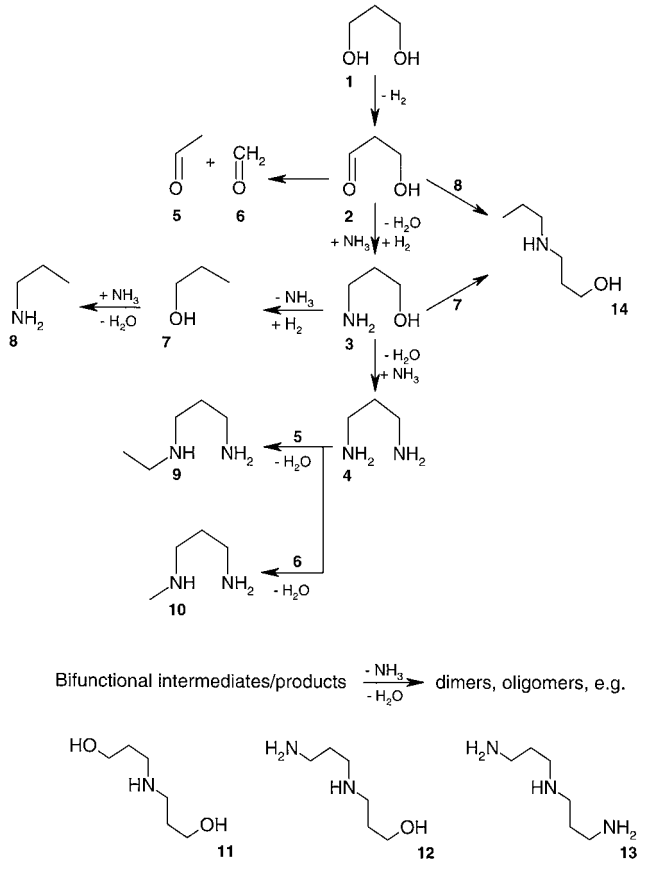

SCHEME 2. Important reactions occurring in the amination of 1,3-propanediol with ammonia. The intermediates and products (except **2**, **5**, and **6**) were identified by GC–MS.

deactivated within a few hours, contained both α- and β-Co phases, and the proportion of α-Co phase increased parallel with the loss of activity. Moreover, both α- and β-Co phases existed in Co–La and Co–Fe treated with acidic or basic salts. These three catalysts afforded considerably lower selectivities and yields of **4**. A further increase in iron content from 5 to 48 wt% (Co–Fe-48) led to the formation of a Co–Fe alloy (Wairauite), and this catalyst was also less efficient than Co–Fe. Apparently, the small amount of Fe additive can stabilize the metastable β-Co phase, and the presence of this single phase in the bulk seems to be a key requirement for obtaining a stable and selective catalyst.

Role of Surface Basic and Acidic Sites

Treatment of the best catalyst Co–Fe prior to drying and calcination with aqueous NaOAc or $(NH_4)_2HPO_4$ was found to be detrimental to catalytic performance with respect to a broad range of reaction parameters. A feasible explanation for the negative influence of strong acidic and basic surface sites is based on a careful analysis of the reactions shown in Scheme 2. The main reaction path leading from **1** to **4** includes metal-catalyzed redox and acid/base-catalyzed condensation (addition–elimination) reactions. A former investigation of the amination of monofunctional aliphatic alcohols (49) demonstrated that the overall reaction rate was limited by the abstraction of an α-hydrogen. This is the first elementary step during dehydrogenation of the alcohol to the corresponding aldehyde. Assuming that the amination of an alkanediol can be divided into two "independent" amination reactions, we can conclude that the presence of strong acidic or basic sites cannot increase the overall rate of the **1** $\rightarrow$ **4** transformation and, therefore, cannot improve the selectivity to **4**. On the contrary, these acidic and basic sites can accelerate the retro-aldol reaction leading to **5** and **6**, the alkylation reactions resulting in **7**–**10** and **14**, and dimerization and oligomerization reactions affording nonvolatile by-products.

The preparation conditions for Co, Co–Fe, and Co–La (choice of precursors and precipitating agent, deposition at neutral pH, etc.) were designed with the aim of minimizing the concentrations of strong acidic and basic sites on the surface of the final catalyst. It was hoped that the model catalysts Co–Fe–Na and Co–Fe–PO_4 would differ from Co–Fe only by the presence of surface basic and acidic sites and would enable us to confirm the above concept. Unexpectedly, even the minor changes during preparation [adsorption of NaOAc or $(NH_4)_2HPO_4$ from dilute aqueous solutions, followed by careful removal of excess salts with hot water] resulted in remarkable changes in the physicochemical properties. The different properties (excluding the acid/base properties) of Co–Fe after modification are illustrated in Tables 2 and 3 and Figs. 1–3. It is probable that the poor catalytic performance of Co–Fe–Na and Co–Fe–PO_4 (Fig. 5) is partly due to these "structural" effects. Especially in the case of Co–Fe–PO_4, the significant amount of α-Co phase and the partial transformation of surface oxide to inactive phosphate during calcination may also contribute to the detrimental influence of phosphate on the catalyst surface.

CONCLUSION

The amination of 1,3-propanediol with ammonia was carried out in a continuous fixed-bed reactor in the temperature range 150–210°C and total pressure range 50–150 bar. Promotion of the unsupported cobalt catalyst with iron or lanthanum improved diamine selectivity significantly. Best catalytic results were obtained with a 95 wt% Co–5 wt% Fe catalyst containing only very weak acidic sites. The active metastable β-cobalt phase tends to transform to the thermodynamically more stable α-cobalt phase under reaction conditions. Addition of a small amount of iron suppresses this transformation, providing stable cobalt catalysts. The absence of strong acidic and basic sites on the catalyst was found to be crucial for the production of 1,3-diaminopropane and for the suppression of various

undesired reactions (retro-aldol reaction, hydrogenolysis, alkylation, disproportionation, dimerization, oligomerization) occurring in the reaction system. The use of supercritical ammonia as solvent and reactant proved to be beneficial for formation of both amino alcohol and diamine. This selectivity enhancement in the near-critical region may be attributed to elimination of the interfacial mass transfer leading to a higher surface concentration of ammonia.

The feasibility of a one-step synthesis of 1,3-diaminopropane from 1,3-propanediol in supercritical ammonia has been demonstrated. Considering the large number of elementary steps involved in this consecutive reaction series, the best yields of 32% for the diamine and 8% for the valuable intermediate amino alcohol are attractive values. The excellent stability of the best Co–Fe catalyst—no significant deactivation up to 10 days on stream—is also a promising feature of the process. However, a substantial further improvement in catalyst composition is required to achieve yields useful for technical application.

ACKNOWLEDGMENTS

Thanks are due H. Bruder of Hoffmann–LaRoche Ltd., Kaiseraugst, Switzerland, for studies of the phase behavior of the reaction mixtures. Financial support from Lonza Ltd, Visp, Switzerland, is kindly acknowledged.

REFERENCES

1. Glaser, H., *in* "Methoden der Org. Chem. (Houben-Weyl)" (E. Müller, Ed.), Vol. XI/1, p. 112. Georg Thieme, Stuttgart, 1957.
2. Herman, R. G., *in* "Catalytic Conversion of Synthesis Gas and Alcohols to Chemicals" (R. G. Herman, Ed.), p. 433. Plenum, New York/London, 1984.
3. Heilen Mercker, H. J., Frank, D., Reck, R. A., and Jäckh, R., *in* "Ullmann's Encycl. Ind. Chem." (B. Elvers, S. Hawkins, M. Ravenscroft, J. F. Rounsaville, and G. Schulz, Eds.), Vol. A2, p. 23. Chemie, Weinheim, 1985.
4. Baiker, A., and Kijenski, J., *Catal. Rev. Sci. Eng.* **27**, 653 (1985).
5. Vogt, P. F., and Gerulis, J. J., *in* "Ullmann's Encycl. Ind. Chem." (B. Elvers, S. Hawkins, M. Ravenscroft, J. F. Rounsaville, and G. Schulz, Eds.), Vol. A2, p. 37. Chemie, Weinheim, 1985.
6. Deeba, M., Ford, M. E., and Johnson, T. A., *in* "Catalysis of Organic Reactions" (D. W. Blackburn, Ed.), Vol. 40, p. 241. Marcel Dekker, New York, 1990.
7. Roundhill, D. M., *Chem. Rev.* **92**, 1 (1992).
8. Turcotte, M. G., and Johnson, T. A., *in* "Kirk–Othmer Encycl. Chem. Technol." (F. M. Mark, D. F. Othmer, C. G. Overberger, and G. T. Seaborg, Eds.), Vol. 2, p. 369. Wiley, New York, 1992.
9. Visek, K., *in* "Kirk–Othmer Encycl. Chem. Technol." (F. M. Mark, D. F. Othmer, C. G. Overberger, and G. T. Seaborg, Eds.), Vol. 2, p. 405. Wiley, New York, 1992.
10. Amini, B., *in* "Kirk–Othmer Encycl. Chem. Technol." (F. M. Mark, D. F. Othmer, C. G. Overberger, and G. T. Seaborg, Eds.), Vol. 2, p. 426. Wiley, New York, 1992.
11. Baiker, A., *in* "Catalysis of Organic Reactions" (J. R. Kosak and T. A. Johnson, Eds.), Vol. 53, p. 91. Marcel Dekker, New York, 1994.
12. Mallat, T., and Baiker, A., *in* "Handbook of Heterogeneous Catalysis" (G. Ertl, H. Knözinger, and J. Weitkamp, Eds.), Vol. 5, p. 2334. VCH Verlagsgesellschaft, Weinheim, 1997.
13. Schreyer, R., U.S. Patent 2,754,330 (1952).
14. Winderl, S., Haarer, E., Corr, H., and Hornberger, P., U.S. Patent 3,270,059 (1966).
15. Adam, K., and Haarer, E., U.S. Patent 3,520,933 (1970).
16. Boettger, H., Hoffmann, H., Toussaint, H., and Winderl, S., U.S. Patent 4,014,933 (1977).
17. Best, D. C., U.S. Patent 4,111,840 (1978).
18. Best, D. C., U.S. Patent 4,123,462 (1978).
19. Jobson, E., Baiker, A., and Wokaun, A., *J. Mol. Catal.* **60**, 399 (1990).
20. March, J., "Advanced Organic Chemistry—Reactions, Mechanisms, and Structure," p. 898. Wiley, New York, 1992.
21. Sirokmán, G., Molnár, Á., and Bartok, M., *J. Mol. Catal.* **19**, 35 (1983).
22. Kijenski, J., Niedzielski, P. J., and Baiker, A., *Appl. Catal.* **53**, 107 (1989).
23. Fischer, A., Mallat, T., and Baiker, A., *Catal. Today* **37**, 167 (1997).
24. Vultier, R. E., Baiker, A., and Wokaun, A., *Appl. Catal.* **30**, 167 (1987).
25. Fischer, A., Mallat, T., and Baiker, A., *Angew. Chem. Int. Ed.* **38**, 351 (1999).
26. Smiley, R. A., *in* "Ullmann's Encycl. Ind. Chem." (B. Elvers, S. Hawkins, M. Ravenscroft, J. F. Rounsavielle, and G. Schulz, Eds.), Vol. A12a, p. 629. Chemie, Weinheim, 1985.
27. Carter, G. C., Doumaux, A. R., Kaiser, S. W., and Umberger, P. R., *in* "Kirk–Othmer Encycl. Chem. Technol." (F. M. Mark, D. F. Othmer, C. G. Overberger, and G. T. Seaborg, Eds.), Vol. 8, p. 74. Wiley, New York, 1992.
28. Maciejewski, M., Müller, C. A., Tschan, R., Emmerich, W. D., and Baiker, A., *Thermochim. Acta* **295**, 167 (1997).
29. Maciejewski, M., Emmerich, W. D., and Baiker, A., *J. Therm. Anal. Cal.*, in press.
30. Allamagny, P., "Encyclopedie de Gaz," p. 951. L'Air Liquide, Elsevier, Amsterdam, 1976.
31. Pelavin, M., Hendrickson, D. N., Hollander, J. M., and Jolly, W. L., *J. Phys. Chem.* **74**, 1116 (1970).
32. McIntyre, N. S., and Cook, M. G., *Anal. Chem.* **47**, 2208 (1975).
33. Hirokawa, K., Honda, F., and Oku, M., *J. Electron Spectrosc.* **6**, 333 (1975).
34. Wagner, C. D., Davis, L. E., Zeller, M. V., Taylor, J. A., Raymond, R. M., and Gale, L. H., *Surf. Interface Anal.* **3**, 211 (1981).
35. Castner, D. G., and Watsin, P. R., *in* "Catalyst Characterization Science: Surface and Solid State Chemistry, Philadelphia, Pennsylvania, August 26–31, 1984" (M. L. Deviney and J. L. Gland, Eds.), Vol. 288, p. 144. ASC, Washington, DC, 1985.
36. Hofer, L. J. E., and Peebles, W. C., *J. Am. Chem. Soc.* **69**, 2497 (1947).
37. Emmett, P. H., and Shultz, J. F., *J. Am. Chem. Soc.* **51**, 3249 (1929).
38. Fukuda, Y., and Rabalais, J. W., *J. Electron Spectrosc. Relat. Phenom.* **25**, 237 (1982).
39. Davydov, A. A., "Infrared Spectroscopy of Adsorbed Species on the Surface of Transition Metal Oxides." Wiley, Chichester 1990.
40. Jobson, E., Dissertation, Laboratory of Technical Chemistry, ETH-No. 8974, Zürich, 1989.
41. Jobson, E., Baiker, A., and Wokaun, A., *J. Chem. Soc. Faraday Trans.* **86**, 1131 (1990).
42. Ramis, G., Busca, G., Lorenzelli, V., and Forzatti, P., *Appl. Catal.* **64**, 243 (1990).
43. Baiker, A., Monti, D., and Fan, Y. S., *J. Catal.* **88**, 81 (1984).
44. Labadie, J. W., and Dixon, J. J., *J. Mol. Catal.* **42**, 367 (1987).
45. Ford, M. E., and Johnson, T. A., *in* "Catalysis of Organic Reactions" (D. W. Blackburn, Ed.), Vol. 40, p. 219. Marcel Dekker, New York, 1989.
46. Corbin, D. R., Schwarz, S., and Sonnichsen, G. C., *Catal. Today* **37**, 71 (1997).
47. Savage, P. E., Gopalan, S., Mizan, T. I., Martino, C. J., and Brock, E. E., *AIChE J.* **41**, 1723 (1995).
48. Baiker, A., *Chem. Rev.* **99**(2), 453 (1999).
49. Baiker, A., Caprez, W., and Holstein, W. L., *Ind. Eng. Chem. Prod. Res. Dev.* **22**, 217 (1983).